

Journal of Quantitative Spectroscopy & Radiative Transfer

www.elsevier.com/locate/jqsrt

Full Length Article

Modulation of Apparent Optical Properties Using Arrayed Mesoscale Structures

David L. Simeroth, Peter A. Kottke, Onur A. Kucuktas, Andrei G. Fedorov¹

George W. Woodruff School of Mechanical Engineering, 801 Ferst Dr, Georgia Institute of Technology, Atlanta, GA 30332

Abstract

In this study, a method for using arrays of mesoscale structures to modify the apparent optical properties of an opaque composite surface has been theoretically demonstrated to both raise and lower the apparent emissivity as compared to the intrinsic properties of the constitutive materials. For design problems where thermomechanical and optical material properties are both of importance, mesoscale surface structuring can greatly expand the design space. Analysis via the net radiosity method herein illustrates the ability to achieve a wide range of spectral apparent optical properties. Notably, a hexagonal array of spheres on a planar surface can raise the apparent emissivity of a planar surface by 50%. Conversely, a hexagonal enclosure of reradiating surfaces, realized by thin adiabatic walls, can reduce the apparent emissivity of a blackbody by half. As this method of modifying apparent optical properties utilizes structures much larger than the wavelengths of interest, the relationship between intrinsic planar emissivity, geometry, and apparent emissivity can be computed semi-analytically at low computational expense. Passive solar cooling, thermophotovoltaic cells, aerodynamic surfaces exposed to intense heating, and solar absorbers are presented as case studies that could benefit from the use of mesoscale structures on opaque surfaces to modify the apparent optical properties.

Keywords: Mesoscale Structures, Apparent Optical Properties, Net Radiosity

1. Introduction

Surface modifications can enhance material thermal performance by altering critical apparent radiative properties. These surface modifications may either be in the form of a material coating with desirable radiative properties, structural modifications of the surface, or both, in order to produce a surface yielding apparent optical properties differing from their constituents' intrinsic optical properties. Structural modifications may further be classified based on different length scales of the modifications themselves, as illustrated in Figure 1. Mesoscale structures are larger than the wavelength of incident radiation ($\lambda \ll D$) and the radiation exchange may be modeled with rays rather than waves, and therefore the analysis of their behavior does not need to

¹ Corresponding Author: AGF@gatech.edu (A. G. Fedorov).

consider diffraction and interference effects (Figure 1b). However, these arrayed structures are still much smaller than the lateral extent of the surface whose apparent optical properties are targeted for modification ($L \ll W$), such that the entire surface may be analyzed as an infinite array of repeating unit cells. Such mesoscale structures provide less flexibility in spectral control over optical behavior than wavelength or sub-wavelength scale metamaterials exploiting the structure-dependent plasmonic resonances, i.e., Figure 1(a), but nevertheless can achieve a significant change (up/down) in the magnitude of the apparent radiative properties for the practically robust surface, which can be realized with simpler manufacturing processes. Mesoscale structures can modify *spectral* behavior because they can use two or more materials with different spectral dependence of their intrinsic optical properties. The modification in light interactions with the surface is a function of the material properties, shape of the repeating structure, and arrangement of the structures on the surface. Because the structures are greater in size than the wavelengths of interest, the interaction can be predicted using the net radiosity method, but extended to treatment of periodic structure arrays.

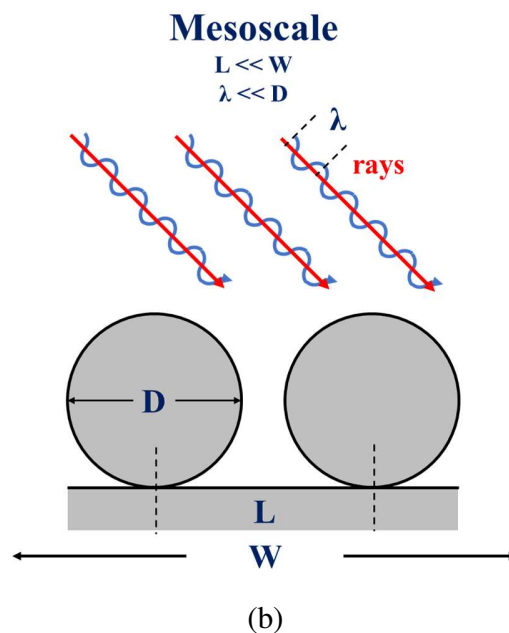
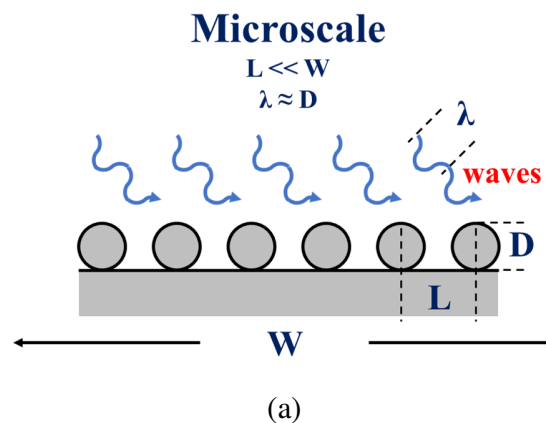


Figure 1: Different scales of surface structuring for optical property modulation. In both cases, the size of the repeating structures (L) is much smaller than the extent of the surface (W) whose optical properties are targeted for modification. (a) Microscale structures with features of the same scale (D) as the wavelengths of interest (λ). Wave nature of radiation needs to be accounted for through non-linear diffraction and interference effects. (b) Mesoscale structures (the focus of this study) has structural features (D) larger than the wavelengths of interest (λ). The radiation exchange may be treated using the linear ray optics through the view factors.

The design of classical optical metamaterials typically relies on electromagnetic radiation field modulation on length scales similar to those of the wavelengths of interest. The apparent optical properties resulting from these plasmonic interactions are functions of frequency, polarization, and incident/emitted angles [1,2]. The specificity of these responses makes them useful for a wide range of applications [3–5]. Examples include passive solar cooling devices, where metamaterials can alter the apparent emissivity spectrum to be low in the visible range and high in the IR range for improved cooling efficiency; [6] thermophotovoltaic (TPV) cells, which see a large increase in efficiency from band-edge spectral filtering; [7] concentrated solar absorbers, where spectral selectivity allows the metamaterial to maintain stability at high temperatures, [8,9] and microscale absorber coatings allow for extremely high solar absorbance; [10] and all-optical analog computing elements, which need to have different responses in different spectral regions, depending on the element. [11]

Alternatively, opaque diffuse structures much larger than radiation wavelengths of interest could also be arranged to modify the apparent optical properties. Such structured surfaces are already used in applications where control of apparent optical properties over the entire spectrum is desired, rather than specific optical properties in specific wavelength regimes. A classic example is a blackbody furnace, wherein the goal of the structure is to dramatically increase the apparent emissivity of the constituent material across the entire spectrum, using a large internal enclosed surface with a small aperture to simulate a blackbody. [12] The lack of plasmonic interactions greatly reduces the complexity of the phenomena: the structures are no longer tailorable for specific directions, wavelengths, and polarizations, but can be analyzed with the net radiosity equations at low computational cost. Further, mesoscale structures benefit from relative ease of manufacturing, especially in applications requiring surface modification over larger areas. Spectral modification of apparent optical properties is achieved with mesoscale structures by the combination of materials with spectral features of interest, and use of the geometric arrangement of the structural elements to amplify or diminish the contributions of intrinsic properties of the constituent materials. Recently, the use of multi-scale, coral-like structures has been used to greatly increase the apparent absorptivity compared to a planar surface, [13] and multi-scale honeycomb structures to minimize heat losses of concentrated solar absorbers. [14,15] This motivates the further understanding and development of predictive tools for the modulation of apparent optical properties for structures of mesoscale dimensions.

This article describes the use of mesoscale surface structuring to control apparent optical properties beyond increasing the apparent emissivity across the entire spectrum. Specifically, this study examines the use of external structures in the form of spheres arranged in a hexagonal array, reradiating surfaces arranged in a honeycomb pattern, and combinations of the former elements made of combination of materials with different spectral emissivity. Addition of an array of spheres generally increases the apparent emissivity, addition of reradiating surfaces

generally reduces the apparent emissivity, and using a combination of materials allows for also changing the spectral behavior of apparent properties. In practice, a reradiating surface array can be realized by forming adiabatic walls on top of the substrate that are tall, thin, and of a low thermal conductivity, minimizing the energy loss through the conjugate heat transfer.

By treating a meso-structured surface as an infinite periodic array of unit cell enclosures, the apparent optical properties of the surface are given by those of the unit cell. The net radiosity method is used to produce semi-analytical relationships between the apparent emissivity, the geometry of the structures via the view factors, and the intrinsic optical properties of the materials used for different surface elements. The analysis presented in this paper was conducted for structured surfaces with spheres arrayed hexagonally on a planar substrate, separated by reradiating surfaces (vanishingly thin walls). The substrate and sphere materials were chosen with a combination of intrinsic optical properties to illustrate the capability for spectral tuning of the apparent emissivity of the composite structure.

In Section 2, we briefly introduce the method of analysis and present the general trends for apparent emissivity predictions for baseline classes of structured surfaces in terms of view factors between various sub-surfaces of the composite. This includes the development and validation of a method for determining the diffuse view factors between surfaces in an array of repeating unit cells. In Section 3, four different case studies motivated by practical applications are presented to illustrate how surface structuring could beneficially impact the relevant thermal performance characteristics. This includes thermal management of hypersonic vehicles, thermophotovoltaics, passive solar cooling, and solar absorbers. In conclusions, we summarize the key findings and discuss the potential of machine learning (ML) to solve the inverse design problems of mesoscale structured surfaces using the analytical tools we develop in this work as the method to generate the large training datasets for ML applications.

2. Apparent Optical Property Modification via Mesoscale Structures

By treating a structured surface as an infinite array of repeating unit cells, the apparent optical properties of the surface are computed using a radiative enclosure analysis of a representative unit cell. The structured surface array, the unit cell, and an enclosure for hexagonally arranged spheres on a planar substrate are shown in Figure 2. For such an array, a unit cell is formed by a sphere and the hexagonal section of planar substrate centered on the sphere of diameter D and edge-to-edge span of the hexagonal unit cell L . The enclosure would consist of these two emitting surfaces, along with two virtual surfaces. One virtual surface would be the vertical surface extending from the substrate to the height of the top of the sphere, representing the periodicity of the array. This virtual surface, comprised of the six vertical planes, would have a specular reflectivity of unity. The final surface of the enclosure is the apparent area, the same size as planar substrate, completing the enclosure. The topping virtual surface is treated as a blackbody with emissive power of zero. These four surfaces with prescribed intrinsic or virtual radiative properties complete the enclosure. The apparent emissivity of the meso-structure arrayed surface, then, is computed by dividing the radiative heat flux q_a leaving the enclosure

through the apparent area of the topping virtual surface divided by the blackbody emissive power E_b at the temperature of the substrate:

$$\epsilon_{app} = \frac{|q_a|}{E_b} \quad (1)$$

It is important to note that this equation holds both on the total and spectral bases.

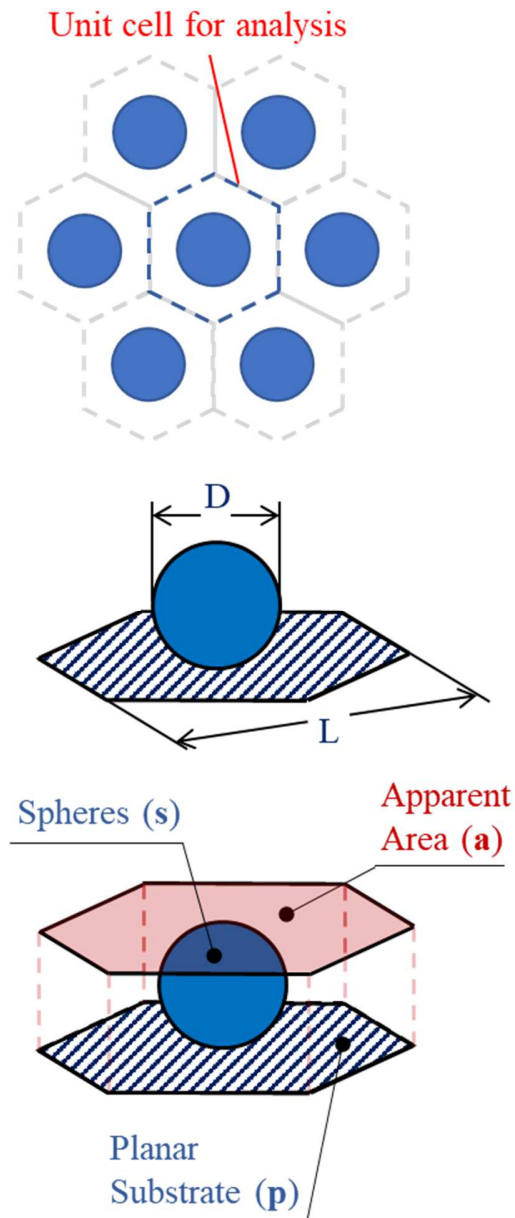


Figure 2: Structured surface comprised of an array of hexagonally packed spheres. Top: Schematic of array, with a single unit cell highlighted. Middle: Schematic of a single unit cell, with relevant geometric parameters shown: L is

the edge-to-edge span of the hexagonal unit cell, and D is the diameter of the spheres. Bottom: Schematic of enclosure used for analysis of radiative exchange in the unit cell. This enclosure includes the isothermal emitting surfaces of the planar substrate and spheres, six vertical virtual surfaces representing planes of symmetry (perfect specular reflectors), and a topping surface representing the apparent area of the unit cell.

2.1. Calculation of View Factors between Infinite Array of Surfaces

Assuming that the substrate surface is isothermal and treating the adiabatic walls as re-radiating surfaces, the blackbody emissive power, radiative heat flux at each surface, and geometry of the enclosure can be related by the system of linear algebraic equations of the net radiosity method. The symmetry boundaries of the unit cell are modeled as “virtual” surfaces which are perfect specular reflectors, giving rise to the specular view factors, to account for cell-to-cell radiative exchange within an infinite array. The partially diffuse partially specular form of the net radiosity method is used to determine the radiative heat flux leaving the enclosure, shown in Equation (2):

$$\frac{q_i}{\epsilon_i} - \sum_{j=1}^N \frac{\rho_j^d}{\epsilon_j} q_j F_{i-j}^s = E_{b,i} - \sum_{j=1}^N (1 - \rho_j^s) E_{b,j} F_{i-j}^s \quad (2)$$

where i and j are indices for iterating through each of the surfaces in the enclosure, N is the number of surfaces in the enclosure, q is the radiative heat flux into the unit cell enclosure through a surface, E_b is the blackbody emissive power, and F_{i-j}^s is the specular view factor from surface i to surface j within the enclosure. The specular view factor is defined as the diffuse energy leaving a surface, intercepted by another surface, by direct travel or any number of specular reflections, divided by the total diffuse energy leaving the first surface.

For diffuse surfaces, $\rho^d = 1 - \epsilon$ and $\rho^s = 0$. For many combinations of surface shapes and orientations, analytical diffuse view factors may be found in [16]. However, a closed form, analytic calculation of diffuse view factors between surfaces in an infinite array of structures of arbitrary size and spacing is not available. Instead, the periodic boundaries of the unit cell are modeled as symmetry boundaries. This may be done by setting the specular reflectivity of the lateral boundaries between the cells to $\rho^s = 1$. However, these specular view factors are also not generally known analytically.

Specular view factors for periodic arrays are a vital aspect of implementing the net radiosity method for determining the apparent optical properties of these mesoscale structures. Monte Carlo simulations [17] were used to determine these view factors. Ray tracing is used to determine whether a given Monte Carlo bundle intersects the sphere, a boundary plane, the substrate, or the apparent area. When a bundle simulated intersects a symmetry plane, that bundle is specularly reflected back into the unit cell, and the intersection is re-calculated, accounting for energy that would have left the unit cell and entered an adjacent cell. This methodology was validated against several limiting cases. A hexagonal unit cell with embedded spheres shows a convergence of the simulated results to the analytical prediction as the sphere radius approaches zero. Similarly, a hexagonal enclosure with purely diffuse bounding surfaces

and a spherical structure agrees well with analytical predictions. Lastly, a hexagonal unit cell with an embedded cylindrical structure, instead of a sphere, shows a convergence of the simulated results of the view factors to the two-dimensional analytical predictions as the height of the unit cell increases. These limiting cases were used to validate the algorithm and to develop the convergence criteria; good agreement (relative error less than 0.1%) was found for simulations with 100,000 bundles.

As the surfaces are all either completely diffuse or completely specular, Equation (2) can then be simplified as follows:

$$\frac{q_i}{\varepsilon_i} - \sum_{j=1}^N \left(\frac{1}{\varepsilon_j} - 1 \right) q_j F_{i-j}^s = E_{b,i} - \sum_{j=1}^N E_{b,j} F_{i-j}^s \quad (3)$$

where F_{i-j}^s is the specular view factor from surface i to surface j within the enclosure, as described above, accounting for the symmetry boundaries.

2.2. Hexagonal Array of Spheres

For an enclosure comprised of a hexagonal array of spheres, the net radiosity method equations are applied to the planar substrate (denoted with p), the sphere (s), and the virtual surface of the apparent area (a). The vertical side walls are treated as perfect specular reflectors, and due to their specular behavior the net radiosity method equation needs to use the specular view factors, as in Equation (3). Solving this system of linear algebraic equations for the heat flux leaving the unit cell through the top surface and normalizing by the emissive power, i.e. applying Equation (1), yields the apparent emissivity of the structured surface:

$$\varepsilon_{app} = \frac{\varepsilon_p (1 - \varepsilon_s) (F_{a-p}^s (1 - F_{s-s}^s) + F_{a-s}^s F_{s-p}^s) + \varepsilon_s (1 - \varepsilon_p) (F_{a-s}^s + F_{a-p}^s F_{p-s}^s) + \varepsilon_p \varepsilon_s (F_{a-p}^s + F_{a-s}^s)}{1 - F_{s-s}^s (1 - \varepsilon_s) - F_{p-s}^s F_{s-p}^s (q - \varepsilon_p - \varepsilon_s + \varepsilon_p \varepsilon_s)} \quad (4)$$

For a configuration where the planar substrate and the sphere are comprised of the same material with the same optical properties, the relationship between the intrinsic properties, the geometry, and the apparent emissivity of the structured surface may be simplified. With identical optical properties, the planar substrate and spheres may be combined into one surface, denoted by e for the entire emitting surface. This simplifies the analysis significantly, yielding the relationship for apparent emissivity shown in Equation (5):

$$\varepsilon_{app} = \frac{1}{F_{e-e}^s + \frac{1}{\varepsilon_e} (1 - F_{e-e}^s)} \quad (5)$$

In this configuration, the specular view factor is a function only of two geometric parameters: the edge-to-edge span of the hexagonal unit cell and the diameter of the spheres, defined in Figure 2. The equation relating intrinsic planar emissivity to apparent emissivity for this class of

structures, then, is a function only of the parameter, D/L , which can vary from 0 to 1. It is shown in Figure 3 as a function of relative sphere size. Increasing the relative size of the sphere increases the relative emitting area to apparent area ratio, thus increasing the apparent emissivity compared to the intrinsic planar emissivity. This effect is more pronounced at lower intrinsic emissivity values and diminishes at higher intrinsic emissivity values, with a blackbody seeing no effect from surface structuring.

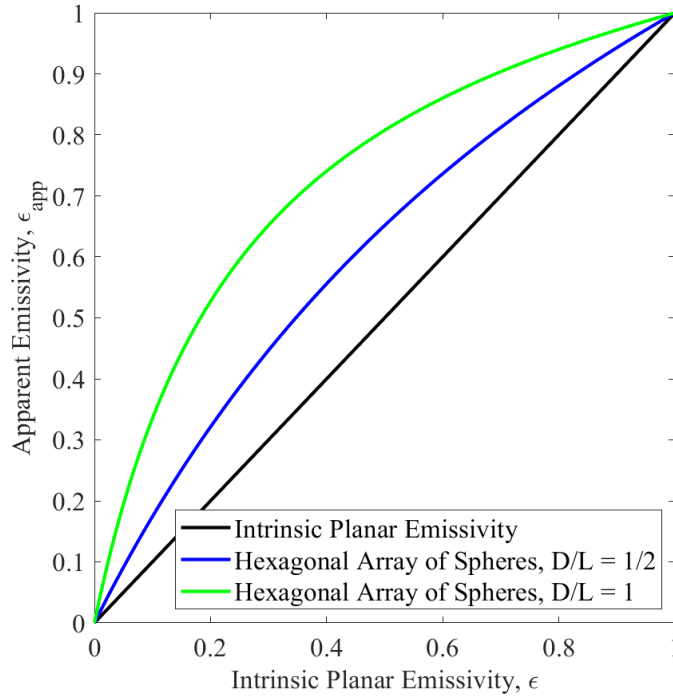


Figure 3: Apparent emissivity as a function of intrinsic planar emissivity for hexagonally packed spheres on a planar substrate, where the substrate and spheres have the same intrinsic emissivity.

2.3. Hexagonal Array of Reradiating Surfaces

For an enclosure comprised of a hexagonal arrangement of reradiating surfaces as shown in Figure 4, the net radiosity method is applied to the planar substrate (denoted with p), the reradiating surfaces (denoted w , for wall), and the virtual (top) surface of the apparent area (a). Just as in the previous case, we are left with three equations and three unknowns from the net radiosity method equation, but in this case the heat flux entering the enclosure through the reradiating surfaces is known (zero), and the blackbody emissive power of the reradiating surfaces are unknown. Solving this system for the heat flux leaving the enclosure through the apparent area and normalizing by the emissive power of the emitting surfaces yields the apparent emissivity:

$$\epsilon_{app} = \frac{1 + F_{p-a}}{2 + (1 + F_{p-a}) \left(\frac{1}{\epsilon_p} - 1 \right)} \quad (6)$$

Where F_{p-a} is the diffuse view factor from the planar substrate to the apparent (topping) area and ϵ_p is the intrinsic emissivity of the planar substrate material. It is important to note that this function necessarily yields an apparent emissivity lower than that of the intrinsic planar emissivity of the substrate. In the limit where $F_{p-a} = 0$ for infinitely tall reradiating surfaces, the lower limit for the apparent emissivity is 1/2 for a black substrate.

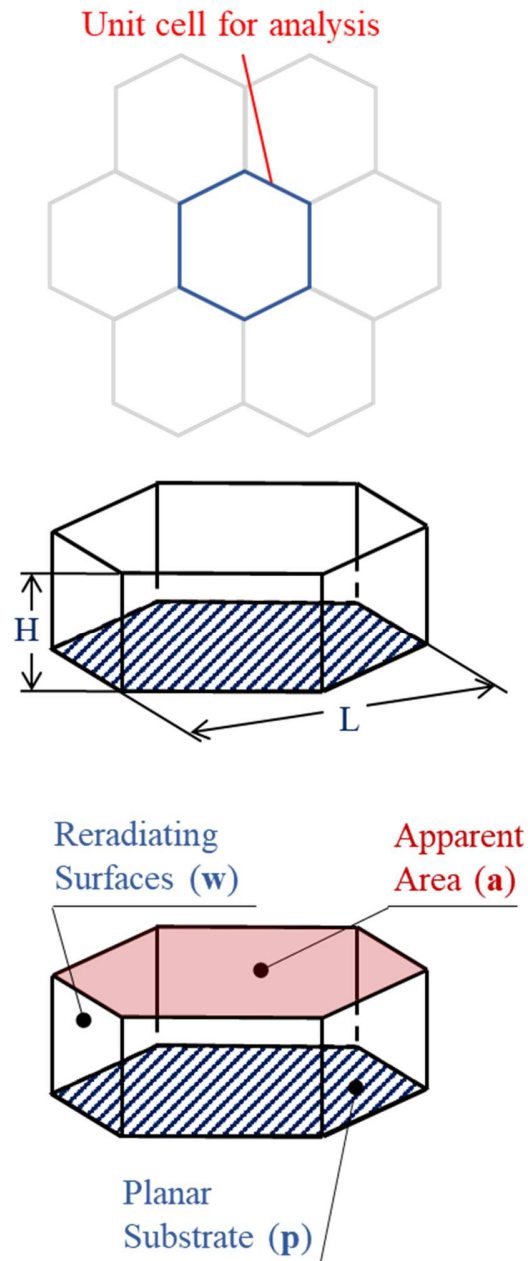


Figure 4: Structured surface comprised of a hexagonal arrangement of reradiating surfaces. Top: Schematic of array, with a single unit cell highlighted. Middle: Schematic of a single unit cell, with relevant geometric parameters shown – L is the edge-to-edge span of the unit cell, and H is the height of the reradiating surfaces.

Bottom: Schematic of enclosure representing the unit cell. This enclosure includes the six reradiating walls, the planar substrate, and a virtual (topping) surface representing the apparent area.

Once again, the governing view factor is a function only of two geometric parameters: the side-to-side span of the hexagonal unit cell, L , and the height of the reradiating surfaces, H , as defined in Figure 4. The relationship between intrinsic planar emissivity to apparent emissivity for this class of structures is a function only of the parameter, H/L , which can vary from 0 to infinity and shown in Figure 5. Increasing the relative size of the reradiating surfaces decreases the view factor from the emitting surface to the apparent area, thus decreasing the apparent emissivity compared to the intrinsic planar emissivity. This effect is more pronounced at higher intrinsic emissivity values, and diminishes at lower intrinsic emissivity values, with a perfect reflector seeing no effect from the reradiating surfaces, and a blackbody's apparent emissivity reduced by as much as half.

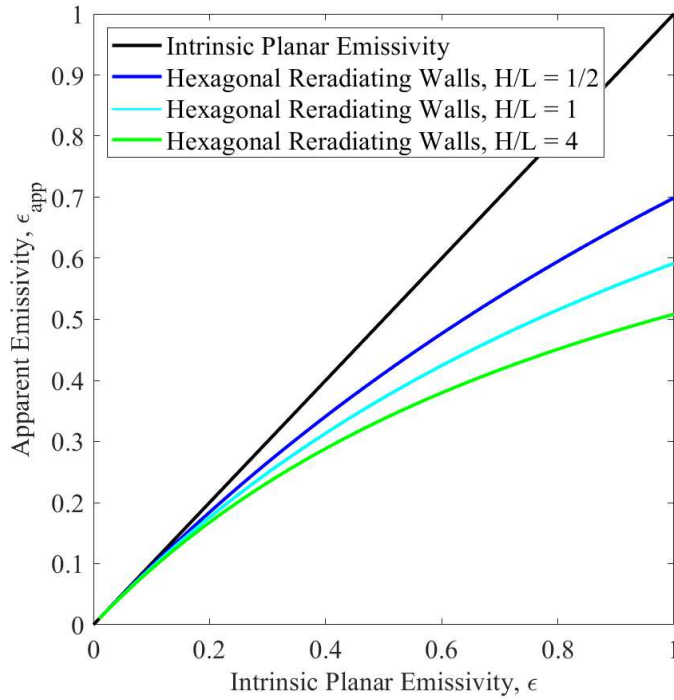


Figure 5: Apparent emissivity as a function of intrinsic planar emissivity for a hexagonal arrangement of reradiating surfaces on a planar substrate.

2.4. Composite Structures

With spheres able to raise the apparent emissivity of a planar material and reradiating surfaces able to lower the apparent emissivity of a planar material, a combination of reradiating surfaces and spheres can achieve a wide range variation, up and down, of possible apparent emissivity values. Figure 6 shows the arrangement of such composite structures, a single unit cell, and an enclosure. With reradiating surfaces, spheres, a planar substrate, and a topping surface with an apparent area to complete the enclosure, the apparent emissivity for this arrangement is solved once more using the net radiosity method equations, Equation (3). Specifically for the case where

the height of the reradiating surfaces is lower than the diameter of the spheres, the portion of the vertical surfaces between the top of the reradiating surfaces and the top of the enclosure is treated as a virtual (symmetry) surface with a specular reflectivity of one. Similar to the hexagonally packed array of spheres, in this arrangement, the diffuse view factors for the reflecting virtual surfaces are replaced by the specular view factors, accounting for reflections off these virtual surfaces.

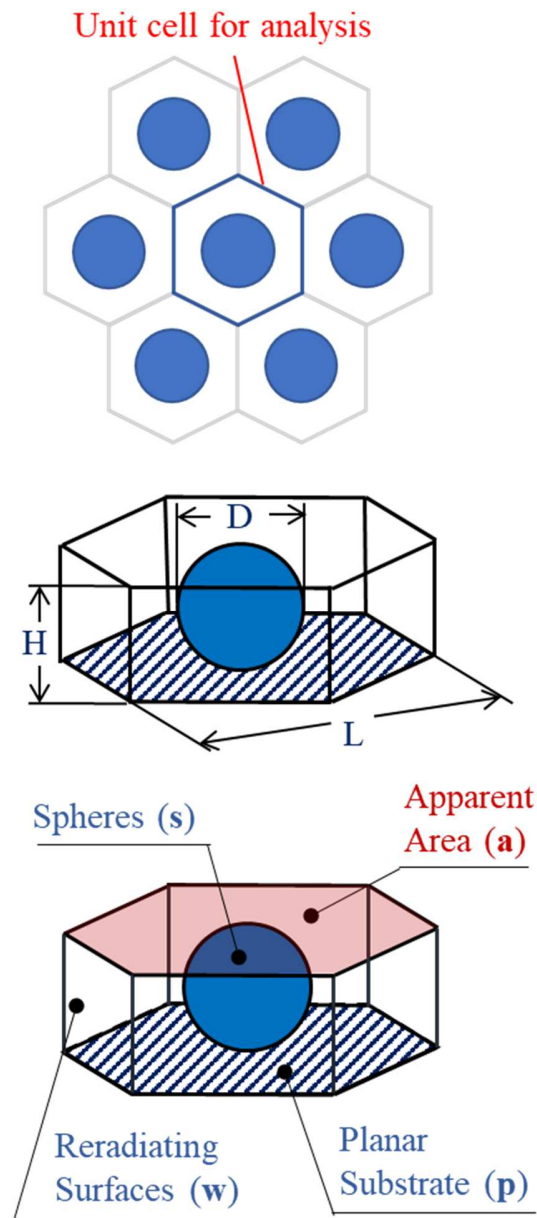


Figure 6: Structured surface comprised of a hexagonal arrangement of cells with walls formed by reradiating surfaces and spheres within them. Top: Schematic of array, with a single unit cell highlighted. Middle: Schematic of a single unit cell, with relevant geometric parameters: L is the edge-to-edge span of the unit cell, D is the diameter of the spheres, and H is the height of the reradiating surfaces. Bottom: Schematic of enclosure representing the unit cell. This enclosure includes the six reradiating walls, the planar substrate, and a virtual (topping) surface

representing the apparent area. For configurations where the reradiating surfaces are smaller in height than the sphere diameter, the remaining wall height segments of the unit cell are defined by virtual surfaces with a specular reflectivity of unity to represent the array symmetry.

Solving for the apparent emissivity of a composite surface of spheres and reradiating walls in a hexagonal arrangement yields a significantly more complex equation:

$$\begin{aligned}
& -\varepsilon_p \varepsilon_s \left(F_{a-p}^s (1 - F_{w-w}^s) + F_{a-w}^s F_{w-p}^s \right) - \varepsilon_s \left(F_{a-s}^s (1 - F_{w-w}^s) + F_{a-w}^s F_{w-s}^s \right) + \dots \\
& \left(\varepsilon_p \varepsilon_s - \varepsilon_p \right) \left(\begin{aligned} & F_{a-p}^s (1 - F_{s-s}^s - F_{w-w}^s - F_{s-w}^s F_{w-s}^s + F_{s-s}^s F_{w-w}^s) + \dots \\ & F_{a-s}^s F_{s-p}^s (1 - F_{w-w}^s) + F_{a-w}^s F_{w-p}^s (1 - F_{s-s}^s) + \dots \\ & F_{a-s}^s F_{s-w}^s F_{w-p}^s + F_{a-w}^s F_{w-s}^s F_{s-p}^s \end{aligned} \right) + \dots \\
& \left(\varepsilon_p \varepsilon_s - \varepsilon_s \right) \left(\begin{aligned} & F_{a-p}^s F_{p-s}^s (1 - F_{w-w}^s) - F_{a-s}^s F_{p-w}^s F_{w-p}^s + \dots \\ & F_{a-p}^s F_{p-w}^s F_{w-s}^s + F_{a-w}^s F_{w-p}^s F_{p-s}^s \end{aligned} \right) \\
\varepsilon_{app} = & \frac{\left(\varepsilon_s - \varepsilon_p \varepsilon_s \right) F_{p-w}^s F_{w-p}^s - (1 - F_{w-w}^s) + (1 - \varepsilon_s) \left(F_{s-w}^s F_{w-s}^s + F_{s-s}^s (1 - F_{w-w}^s) \right) + \dots}{\left(1 - \varepsilon_p \right) \left(1 - \varepsilon_s \right) \left(\begin{aligned} & F_{p-s}^s F_{s-p}^s (1 - F_{w-w}^s) + F_{p-w}^s F_{w-p}^s (1 - F_{s-s}^s) + \dots \\ & F_{p-s}^s F_{s-w}^s F_{w-p}^s + F_{p-w}^s F_{w-s}^s F_{s-p}^s \end{aligned} \right)} \quad (7)
\end{aligned}$$

In this case, while some of the view factors (those that are zero, and view factors to and from the sphere in configurations where the reradiating surfaces are greater in height than the diameter of the sphere) may be determined analytically, others must be determined numerically, as with the view factors for the hexagonal array of spheres. There are now three geometric parameters - H , L , and D - governing the relationship between the apparent emissivity of the structured surface and the intrinsic emissivities of the sphere and planar substrate. Normalizing by the size of a single unit cell, the two dimensionless geometric parameters, H/L and D/L , can be defined. Figure 7 shows the relationship between the apparent emissivity for a structured surface with differing optical properties for the substrate and sphere, as a function of D/L , at four different reradiating surface heights H/L .

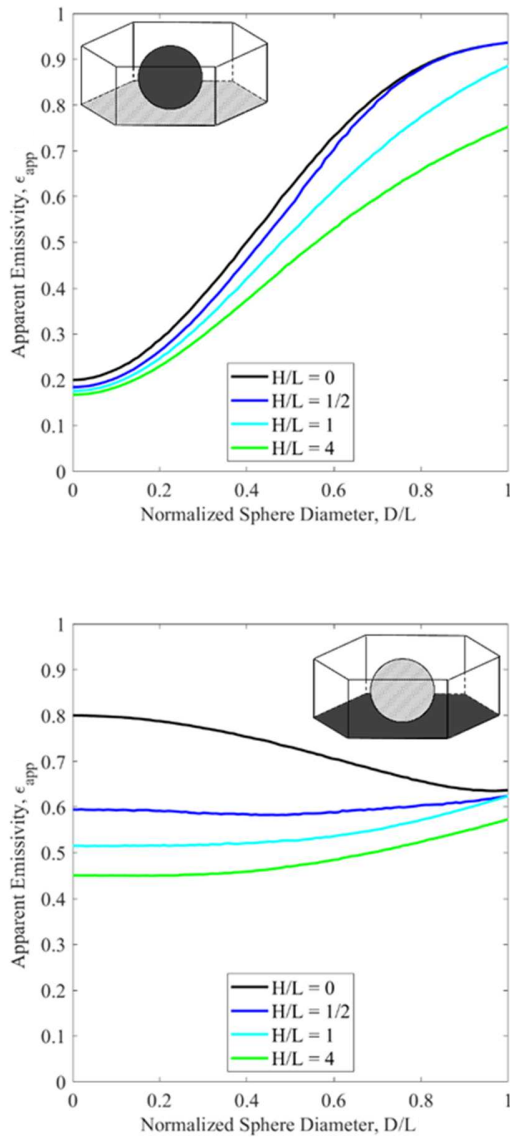


Figure 7: Apparent emissivity of composite structure of a hexagonal arrangement of reradiating surfaces with enclosed spheres on a planar substrate of a different material, as a function of relative sphere diameter. The Monte Carlo method for calculating view factors used 100,000 ray bundles. Top: Highly reflecting substrate ($\epsilon = 0.2$), reradiating surfaces (agnostic to the material properties), and high absorptivity spheres ($\epsilon = 0.8$). Bottom: High absorptivity substrate ($\epsilon = 0.8$), reradiating surfaces (agnostic to the material properties), and highly reflecting spheres ($\epsilon = 0.2$).

Both reradiating surfaces and the inclusion of more reflecting spheres can reduce the apparent emissivity of the substrate. The impact of reradiating surfaces alone can be observed by considering the behavior in Figure 7 at a normalized sphere diameter (D/L) of zero. For a highly reflective substrate surface, shown in Figure 7 top, the achievable reduction in apparent emissivity is modest. But for a less reflecting (high emissivity) substrate, shown in Figure 7 bottom, the achievable reduction in apparent emissivity with reradiating surfaces is significant, and in fact, is greater than it would be possible to achieve with the inclusion of reflective spheres. The greatest effect of including the spheres is seen in Figure 7 (top) when $D/L = 1$: the

apparent emissivity can be made above or below the intrinsic emissivity of the spheres by about 10% by varying the relative height of the reradiating surfaces. This is a significant general result that is worth to emphasize. With the combination of reradiating surfaces (adiabatic walls) and embedded spheres, it is possible to achieve apparent spectral emissivity values that are lower than the emissivity of the more reflective material, and higher than the emissivity of the more emissive material.

3. Applications Case Studies

When designing any component where thermal, mechanical, and optical phenomenon are of importance, the selected material is often a compromise between desired mechanical properties and desired optical properties. Structured surfaces enable an increase in the available design space by allowing a wider band of achievable optical properties without significantly changing the mechanical properties. Applications where the radiative properties drive the design problem lend themselves well to structured surfaces, such as passive solar cooling, thermophotovoltaic cells, and high-speed aerodynamic surfaces, where high thermal and mechanical loads must be sustained and heat rejection via thermal radiation is desired. To illustrate the effects of mesoscale structuring, a small selection of spectra is presented for these examples.

3.1. Thermal Management of Hypersonic Vehicle

As an example of a surface that would benefit from apparent optical property control, a hypersonic vehicle's external skin material should be capable of withstanding the thermo-mechanical loading of a high-speed aerodynamic environment, as well as having high emissivity for radiative heat rejection, especially in the region of the spectrum corresponding to the maximum spectral blackbody emissive power at the temperature (~1500-2000 K) of the skin. Alumina, especially in the form of a ceramic matrix composite, is well-suited to handle extreme aerodynamic environments. However, as seen in Figure 8, alumina has low emissivity in the visible part of the spectrum. The inclusion of alumina spheres, arranged in a hexagonal pattern, results in a spectral behavior with significantly higher apparent emissivity, especially in the visible spectral range where the planar intrinsic emissivity is low. As reradiating surfaces always result in a decrease of apparent emissivity, they are not desirable for use in this application. By packing the alumina spheres ($D/L = 1$), the apparent emissivity of the structured surface in the visible and near infrared spectral region increases two-fold from 0.35 to 0.7, greatly improving the ability of the surface to reject heat from the hypersonic vehicle at high operating temperatures.

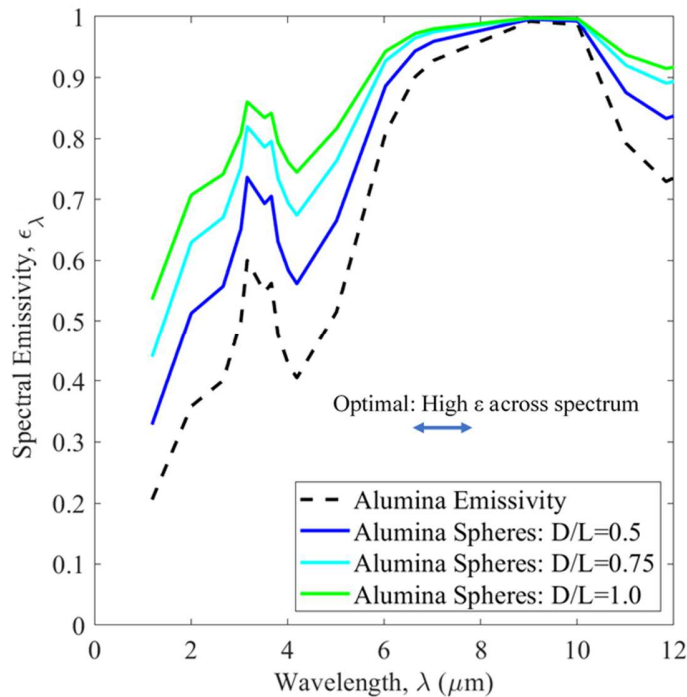


Figure 8: Intrinsic and apparent spectral emissivity of alumina and a class of mesoscale structured surfaces, comprised of alumina spheres on an alumina planar substrate, and without reradiating surfaces (not appropriate for this application). Arrows indicate spectral regions of interest and the desired spectral values for use where the surface will be exposed to hypersonic flow.

3.2. Thermophotovoltaic Cells

For a thermophotovoltaic (TPV) cell, some form of spectral control is required for an efficient system. This can be accomplished with a spectrally selective emitter, an optical filter, a back surface reflector (BSR), or some combination of these. [18] In order to minimize parasitic heating of the TPV receiver (photon-to-electron converter), a BSR would ideally have very high reflectivity (low emissivity) across the spectrum. These reflectors are often comprised of a material with intrinsically low emissivity and high thermal conductivity, such as silver. The reflectivity of the BSR has a strong impact on the efficiency of the entire TPV cell, so ideally, the emissivity of this surface will be as low as possible. Reradiating surfaces can decrease the apparent emissivity of a surface, so a mesoscale structured surface with thin walls arranged in a hexagonal array over a silver substrate would decrease the apparent emissivity, thereby increasing the efficiency of a TPV. With walls four times higher than the span of each unit cell, the apparent emissivity of this surface is decreased by $\sim 3\%$ compared to planar silver, as shown in Figure 9.

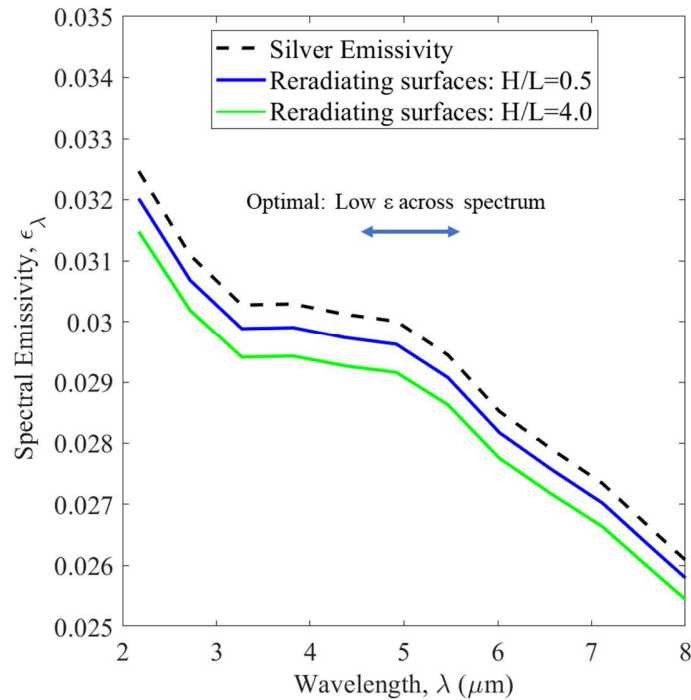


Figure 9: Apparent spectral emissivity of a class of mesoscale structured surfaces, comprised of a silver planar substrate, with reradiating surfaces (separating walls) of varying heights, as compared to the intrinsic emissivity of silver. Arrows indicate spectral regions of interest and the desired spectral values for use in a thermophotovoltaic cell application.

3.3. Passive Cooling from Solar Irradiation

For use in passive cooling from solar irradiation, a surface would ideally have low emissivity (absorptivity) at the wavelengths of the maximum solar emissive power to minimize heat absorption from solar irradiation. This surface would also benefit from high emissivity at the wavelengths of the maximum spectral blackbody emissive power at the surface temperature to maximize heat rejection via radiation. The performance of a given material selection can be quantified by the ratio of an intrinsic material's emissivity to a structured surface's apparent emissivity in the relevant spectral ranges. In the case of a passive solar cooling application, the performance goals are to achieve emissivity reduction in the visible (VIS) spectra and emissivity enhancement in the infrared (IR) spectra.

A simple, structured mesoscale surface comprised of a substrate of polished aluminum with an array of alumina spheres surrounded by the thin, adiabatic walls is used to illustrate the utility of structured surfaces for passive solar cooling. Taking the height of the adiabatic walls at 4 times the center-to-center distance of the unit cells, and varying the diameter of the sphere inside, Figure 10 shows the resulting spectra. Polished aluminum (Al) is highly reflecting broadly across the spectrum, with an intrinsic emissivity between 0.2 and 0.1 in VIS, and below 0.05 in IR. [19] As alumina (Al_2O_3) has a high spectral emissivity in the infrared region and a relatively low spectral emissivity in the visible region, it is chosen as an example to augment the apparent

emissivity of a structured surface comprised of alumina spheres on the aluminum substrate. Increasing the size of the alumina spheres raises the overall apparent emissivity, but also modifies the shape of the emissivity's spectral behavior. At lower D/L values, there is a relatively large increase in spectral emissivity in IR with only a small increase in the apparent emissivity in the visible region. Specifically, at a D/L value of $1/2$, the apparent emissivity (absorptivity) in the visible range increases about two-fold, but the apparent emissivity in the IR region increases by almost 20 times, highlighting the powerful utility of this meso-structured surface for a passive solar cooling application.

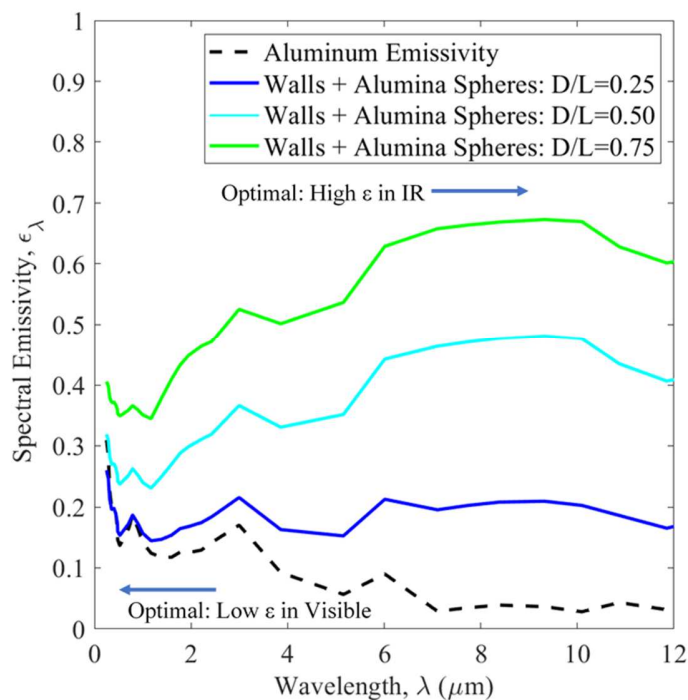


Figure 10: Intrinsic and apparent spectral emissivities of a class of mesoscale structured surfaces, comprised of alumina spheres on an aluminum planar substrate, with reradiating surfaces (separating walls) of relative height $H/L=4$. Arrows indicate spectral regions of interest and the desired spectral values for use in a passive solar cooling application.

3.4. Solar Thermal Collector

As a final example, we consider a solar thermal collector. Ideally, it should absorb as much solar irradiation as possible, with a peak spectral emissive power around $0.5 \mu\text{m}$. Besides the visible region, however, such a surface would optimally have a very low emissivity in the region of the spectrum corresponding to the maximum spectral blackbody emissive power at the collector's operating temperature, to minimize radiative heat losses. Figure 11 shows the emissivity spectrum of silicon as the baseline material. Notably, while silicon has desirably high spectral emissivity (absorptivity) values in the visible regime, it also has relatively high spectral emissivity in the IR region, which is detrimental to the overall thermal collection efficiency. For a limited number of practically suitable metals, semiconductors, and ceramics that we analyzed in an intuition-guided optimization process, no material and geometric parameter combinations of structured surfaces investigated allowed for both raising the visible spectral range apparent

emissivity and depressing the IR apparent emissivity. For example, an arrangement of nickel spheres packed within hexagonal adiabatic walls of height $H/L = 2$ raise the apparent emissivity in the visible range above that of the planar silicon substrate, but at the cost of a similarly increased emissivity in most of the IR region. However, it is possible that an optimal mesoscale structure(s) does exist, but the combination of materials, geometric configurations, and particular geometric parameters to produce such a structured surface would likely only be found through computationally unmanageable “testing” of different parameters and material possibilities. A promising alternative for finding the optimal structured surface is to use the techniques of machine learning (ML), while using the training datasets that can be readily produced using the tools developed in this work from a catalog of materials and mesoscale configurations.

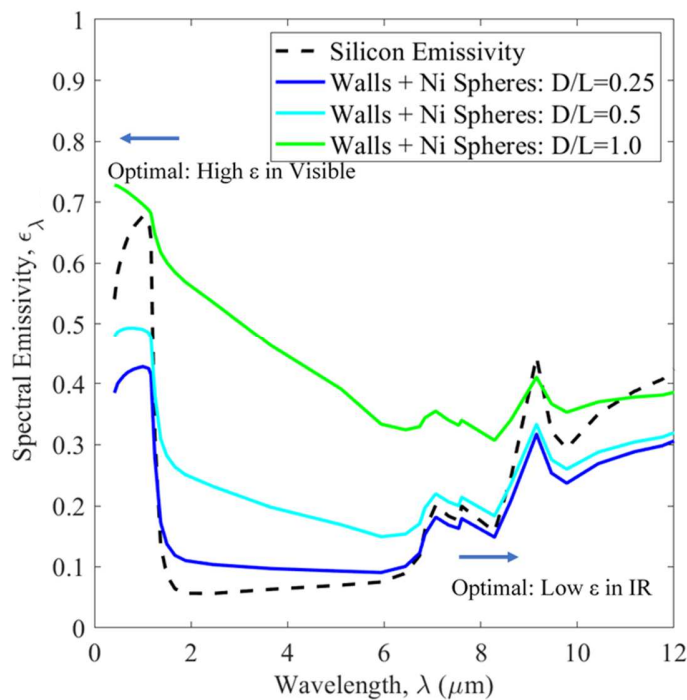


Figure 11: Intrinsic and apparent spectral emissivity of silicon and a class of mesoscale structured surfaces, comprising of alumina spheres on an alumina planar substrate, with reradiating surfaces (adiabatic walls) of height $H/L = 2$. Arrows indicate spectral regions of interest and the desired spectral values for application in a solar thermal collector.

4. Conclusions

The combination of mesoscale spheres and reradiating surfaces arranged in a structured array on top of a planar substrate form a mesoscale structured surface that enables modulation of apparent optical properties over a broad range, in terms of magnitude and spectral behavior. An approach to relating the structure geometry, materials’ intrinsic properties and apparent optical surface properties is implemented at a low computational cost, owing to the semi-analytical solutions of the net radiosity method. In particular, the use of closely packed spheres in a hexagonal array can more than double the apparent emissivity, while incorporation of adiabatic wall structures as reradiating surfaces allows for a decrease in the apparent emissivity of a blackbody substrate by

a factor of two. Additionally, for a choice of the substrate material constrained by other design requirements, the use of a combination of spheres and reradiating surfaces on top of such a substrate are shown to greatly influence the apparent optical properties of the structured surface and selectively raise or lower the spectral properties as needed for different spectral windows. Four application case studies are presented to demonstrate the utility of mesoscale structured surfaces, along with specific examples of selecting the materials and geometric parameters that show a marked improvement in the apparent spectrum compared to the intrinsic optical behavior of a substrate material.

While our analysis considered specifically the hexagonal array structure comprised of opaque diffusely emitting spheres surrounded by reradiating surfaces of adiabatic walls, the approach is general and could be used to determine the relationships between the geometric parameters of any periodic arrays with repeating mesoscale structures and resulting structured surface apparent optical properties. The analytical framework put forth in this article may be utilized to efficiently generate large datasets, which could be useful for the training of machine learning algorithms to optimize the structural features and geometric arrangement of the arrayed composite surfaces resulting in desired apparent radiative properties.

Acknowledgements

This work was performed with Government support under contract number DE-AR0001207 awarded by DOE, Office of ARPA-E. D. Simeroth's work is funded through the Secretary of the Air Force Prestigious Captain's STEM PhD Fellowship. The views expressed in this article are those of the author and do not necessarily reflect the official policy or position of the Air Force, the Department of Defense or the U.S. Government. The insightful discussion and input from Sean Lubner, Ravi Prasher, and Alok Singh (LBNL) helped improve the manuscript.

Declaration of Competing Interest

The authors have no competing interests.

References

- [1] Li W, Fan S. Nanophotonic control of thermal radiation for energy applications [Invited]. *Opt Express* 2018;26:15995. <https://doi.org/10.1364/oe.26.015995>.
- [2] Fan S. Thermal Photonics and Energy Applications. *Joule* 2017;1:264–73. <https://doi.org/10.1016/j.joule.2017.07.012>.
- [3] Blanchard C, Wojszwyk L, Jamois C, Leclercq J-L, Chevalier C, Ferrier L, et al. Metallo-dielectric metasurfaces for thermal emission with controlled spectral bandwidth and angular aperture. *Opt Mater Express* 2022;12:1. <https://doi.org/10.1364/ome.443111>.
- [4] Rubin NA, Shi Z, Capasso F. Polarization in diffractive optics and metasurfaces. *Adv Opt Photonics* 2021;13:836. <https://doi.org/10.1364/aop.439986>.
- [5] Overvig AC, Mann SA, Alù A. Thermal Metasurfaces: Complete Emission Control by Combining Local and Nonlocal Light-Matter Interactions. *Phys Rev X* 2021;11:21050. <https://doi.org/10.1103/PhysRevX.11.021050>.

- [6] Mandal J, Fu Y, Overvig AC, Jia M, Sun K, Shi NN, et al. Hierarchically porous polymer coatings for highly efficient passive daytime radiative cooling. *Science* (80-) 2018;362:315–9. <https://doi.org/10.1126/science.aat9513>.
- [7] Omair Z, Scranton G, Pazos-outón LM, Xiao TP, Steiner MA, Ganapati V. Ultraefficient thermophotovoltaic power conversion by band-edge spectral filtering. *Proc Natl Acad Sci U S A* 2019;116:6. <https://doi.org/10.1073/pnas.1903001116>.
- [8] Wang H, Haechler I, Kaur S, Freedman J, Prasher R. Spectrally selective solar absorber stable up to 900 °C for 120 h under ambient conditions. *Sol Energy* 2018;174:305–11. <https://doi.org/10.1016/j.solener.2018.09.009>.
- [9] Kumar KKP, Mallick S, Sakthivel S. Nanoparticles Based Single and Tandem Stable Solar Selective Absorber Coatings with Wide Angular Solar Absorptance. *Sol Energy Mater Sol Cells* 2022;242:111758. <https://doi.org/10.1016/j.solmat.2022.111758>.
- [10] Lipiński W, Abbasi-Shavazi E, Chen J, Coventry J, Hangi M, Iyer S, et al. Progress in heat transfer research for high-temperature solar thermal applications. *Appl Therm Eng* 2021;184. <https://doi.org/10.1016/j.applthermaleng.2020.116137>.
- [11] Estakhri NM, Edwards B, Engheta N. Inverse-designed metastructures that solve equations. *Science* (80-) 2019;363:1333–8. <https://doi.org/10.1126/science.aaw2498>.
- [12] Cabannes F, Vutien L. A Zirconia Near-Blackbody Radiation Source , 2500 K in Air ~. *Int J Thermophys* 1995;16:277–87.
- [13] Torres JF, Tsuda K, Murakami Y, Guo Y, Hosseini S, Asselineau C-A, et al. Highly efficient and durable solar thermal energy harvesting via scalable hierarchical coatings inspired by stony corals. *Energy Environ Sci* 2022;15:1699–2166. <https://doi.org/10.1039/d1ee03028k>.
- [14] Capuano R, Fend T, Stadler H, Hoffschmidt B, Pitz-Paal R. Optimized volumetric solar receiver: Thermal performance prediction and experimental validation. *Renew Energy* 2017;114:556–66. <https://doi.org/10.1016/j.renene.2017.07.071>.
- [15] Cagnoli M, Froio A, Savoldi L, Zanino R. Multi-scale modular analysis of open volumetric receivers for central tower CSP systems. *Sol Energy* 2019;190:195–211. <https://doi.org/10.1016/j.solener.2019.07.076>.
- [16] Howell J. A Catalog of Radiation Heat Transfer Configuration Factors. *Dep Mech Eng Univ Texas Austin* 2002:302. <http://www.thermalradiation.net/indexCat.html>.
- [17] Modest M. Radiative Heat Transfer. Third Edit. Oxford: Elsevier; 2013. <https://doi.org/10.1016/C2010-0-65874-3>.
- [18] Kazim AH, Asif M, Nadeem K, Shoukat Z, Nazir R, Malik MS, et al. Efficiency Enhancement of a Thermophotovoltaic System Integrated With a Back Surface Reflector. *IEEE Access* 2020;8:153226–39. <https://doi.org/10.1109/ACCESS.2020.3017504>.
- [19] Teodorescu G. Radiative Emissivity of Metals and Oxidized Metals at High Temperature. 2007.